ARTICLE IN PRESS

Journal of Power Sources xxx (xxxx) xxx

Contents lists available at ScienceDirect

Journal of Power Sources

journal homepage: www.elsevier.com/locate/jpowsour

Effect of formation protocol: Cells containing Si-Graphite composite electrodes

Nancy Dietz Rago [1], John K. Basco [1], Anh Vu [1], Jianlin Li [2,**], Kevin Hays [2], Yangping Sheng [2], David L. Wood III [2], Ira Bloom [1,*]

[1] Chemical Sciences and Engineering Division, Argonne National Laboratory, Argonne, IL, 60439, USA
[2] Energy and Transportation Science Division, Oak Ridge National Laboratory, Oak Ridge, TN, 37831, USA

HIGHLIGHTS

- Fast and slow formation protocols were compared in cells with Si/graphite anodes.
- More fluorine was detected on the anode surface of slow-formation-protocol cells.
- No difference in capacity fade rate was seen in these cells.

ARTICLE INFO

Keywords:
Lithium-ion battery
Silicon/graphite anode
Formation protocol

ABSTRACT

The effect of formation protocol was determined in tests using small pouch cells containing silicon-graphite/Li $(Ni_{0.5}Mn_{0.3}Co_{0.2})O_2$ chemistry. The time for the formation protocol was either 13.2 or 186 h for the tested cells. It is demonstrated that the "fast" formation protocol produces cells with similar performance characteristics to that of the "slow" protocol. In addition, the solid-electrolyte interface layers from both formation protocols are stable and function analogously, albeit with different chemistry. The fast formation protocol may thus provide a more economical route to cell fabrication.

1. Introduction

In recent years, lithium-ion batteries (LIBs), which possess an attractive combination of specific energy and power, have been the subject of much development for automotive applications. Battery-powered vehicles containing this technology have been accepted by consumers. However, there is still the problem of limited driving range, possibly causing "range anxiety." Approaches to addressing this problem are to increase the active material ratio (e.g., use thicker electrodes) and utilize higher capacity active materials [1–3].

While graphite is a typical anode in commercial LIBs, many alternative materials have been suggested to further increase cell energy density. Among them is silicon, which has a capacity density of about 3579 mAh g^{-1} when forming $Li_{15}Si_4$ [4], ~10 times higher that of graphite. However, there are many challenges associated with Si anodes, including poor mechanical strength and dramatic volume expansion. To overcome the challenges, silicon is normally synthesized in nanoscale shapes (e.g., nanoparticles [5] and nanotubes [6]) and/or confined in unique structures (e.g., core shell [7] and nanofiber [8]) for high performance. The fine particles and their associated large surface area introduce challenges: 1) they are difficult to disperse and produce significant gas generation [9] and 2) a thick and continuously forming solid-electrolyte interphase (SEI) consumes the lithium, leading to poor cyclability [10] and therefore requiring more electrolyte [11].

After assembly and electrolyte injection, lithium-ion cells must go through a formation process, whereby the electrode materials become electrochemically active. Extensive efforts have been made to understand the SEI morphologies and properties of graphite [12], whereas there is much less study on Si, which is mostly focused on electrolyte composition [13,14]. Usually, the formation process consists of slow charge and discharge steps, with each anode developer using its own, usually, proprietary protocols. The slow cycling adds expense to the product due to the electricity used and lowers the number of cells that can be formed in a given period without a large investment in cycling

* Corresponding author.
** Corresponding author.
E-mail addresses: lij4@ornl.gov (J. Li), ira.bloom@anl.gov (I. Bloom).

https://doi.org/10.1016/j.jpowsour.2019.04.076
Received 11 February 2019; Received in revised form 15 March 2019; Accepted 17 April 2019
Available online 4 June 2019
0378-7753/© 2019 Elsevier B.V. All rights reserved.

Please cite this article as: Nancy Dietz Rago, *Journal of Power Sources*, https://doi.org/10.1016/j.jpowsour.2019.04.076

Table 1
Electrode chemistry.

Cathode	Anode
90 wt% Toda NMC532	15 wt% NanoAmor Si (70–130 nm)
5 wt% carbon black (Imerys, C65)	73 wt% MAG E3 graphite (Hitachi)
5 wt% pVdF (Solvay, 5130)	2 wt% carbon black (Imerys, C45)
Loading: 12.9 mg/cm^{-2}	10 wt% polyacrylic acid (Sigma Aldrich, 450k MW)
Thickness 48 µm	Loading 3.5 mg/cm^2
Porosity: 35%	Thickness: 31 µm
	Porosity: 40%

equipment. It would be more cost-effective to have the formation take the least amount of time without sacrificing battery performance and life [15]. The overall formation process can be shortened by increasing the formation current densities [16] or adopting a shallow charge-discharge voltage window [17] while maintaining identical electrochemical performance for cells with graphite. However, the effect of formation period on the SEI properties and electrochemical performance of silicon/graphite composite anodes has not been reported.

Oak Ridge (ORNL) and Argonne National Laboratories collaborated to determine the effect of formation protocol on performance and life in pouch cells containing Si-graphite anodes. Specifically, we addressed the question of whether cells formed by using C/20 charge and discharge cycles perform better or live longer than those formed using C/5 cycles. After cycling the cells, they were dismantled, and the silicon-graphite electrode was characterized to determine any differences between the effects of the slow and fast protocols.

2. Experimental

2.1. Materials

750-mAh pouch cells were made at the DOE Battery Manufacturing Facility (BMF) at ORNL. The cells contained Si-graphite anodes and Li $(Ni_{0.5}Mn_{0.3}Co_{0.2})O_2$ (NMC532) cathodes. The compositions of these electrodes are given in Table 1. For better slurry wettability, the Al foil was treated by a corona plasma at 4.4 J/cm^2 before coating it on the NMC532 cathode [18]. The electrolyte consisted of 1.2 M $LiPF_6$ in 3:7 ethylene carbonate (EC) and ethyl methyl carbonate (EMC) in a 3:7 ratio (GEN 2) plus 10% fluoroethylene carbonate (FEC) as a co-solvent. Information on materials and electrode fabrication has been reported in previous work [19,20]. The cells were filled with electrolyte to three times the calculated total pore volume.

2.2. Formation and testing

The cells were tap charged to 1.5 V at C/10 and rested for 1 h before subsequent formation protocols were started. The "slow" formation protocol consisted of 5 cycles at C/20 between 4.1 and 3.0 V. The "fast" formation protocol consisted of 5 cycles of constant current and constant voltage at C/5 with a tap current of C/20 between 4.1 and 3.9 V, which was based on the hypothesis that most SEI forms at a high state of charge [17]. After formation, three cells each from the fast and slow formation protocols went through 100 cycles at C/1 charge and discharge between 3 and 4.1 V at 30 °C.

2.3. Post-test analysis

Post-test analysis of the cells was performed to characterize the differences in electrode chemistry and surface morphology that were caused by the two formation protocols. The cells were opened in an argon-atmosphere glove box. Prior to characterization, the anode material was washed two times in excess dimethyl carbonate for 1 min per wash. Sections of the anode material were then characterized by the methods described below.

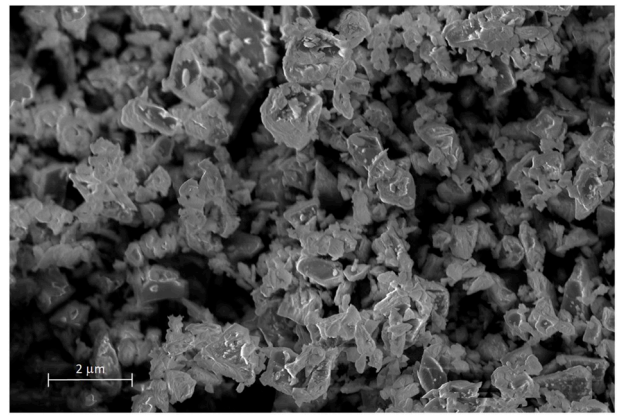

Fig. 1. Scanning-electron image of the silicon used in the cells.

2.3.1. Scanning electron microscopy

A Zeiss Merlin VP at 3 keV was used to characterize the silicon powder at ORNL. Sections of the negative electrodes were cleaned two times by swirling 1 min each in excess dimethyl carbonate. Rinsed pieces of the positive electrodes were placed in an air-tight holder, which was based on a design published by ORNL [21]. The spring-loaded lid was secured with two screws. The sealed assembly was removed from the glove box and subsequently evacuated. After the screws had been removed, the holder was placed in a JEOL JSM-6610LV scanning electron microscope (SEM). In the SEM column, the holder lid was opened when the vacuum in the column exceeded the vacuum inside the holder. Energy-dispersive spectroscopy (EDS) was performed using an Oxford Instruments XMax^N detector (detector size = 50 mm^2) and AZtecEnergy® software.

2.3.2. X-ray photoelectron spectroscopy (XPS)

For surface analysis, XPS of rinsed electrodes was conducted in a Thermo Scientific™ K-Alpha$^+$™ spectrometer by using a micro-focused monochromatic Al-Kα (1487 eV) X-ray source with a spot size of 400 µm. During all surface analyses, a dual-beam electron flood gun (ultra-low energy, 200 eV, co-axial electron and Ar^+ ion beam) was used for charge compensation. Sample preparation was done inside an argon glove box, and the sample was stored in an atmosphere-controlled holder before being loaded into the XPS instrument. The mounted samples were evacuated on the sample stage mount in an isolated load-lock chamber until a base pressure of 3×10^{-7} torr (or lower) was reached. They were then transferred via a pneumatic transfer manipulator arm to the analysis chamber. Operational pressures in the chamber prior to analysis were typically 1 to 4×10^{-9} torr and 2 to 4×10^{-7} torr with the e-flood gun on during surface analysis. Auto-firing, titanium sublimation pump filaments and e-flood gun filaments were degassed prior to analysis. Ar^+-sputtering occurred at 3-keV bombardment voltage at low current, corresponding to an effective etch rate (for a Ta_2O_5 film) of ~0.23 nm s^{-1} and ~1 nm cycle^{-1}. Processing of the spectral data was performed with Thermo Avantage5 (v. 5.977, Build 06436) post-processing software, and charge correction of each spectrum was applied by referencing to the adventitious C1s peak at 284.8 eV.

3. Results

Fig. 1 shows a scanning-electron image of the silicon used in these cells. There was a range of particle sizes and shapes. Although the particle size was reported to be in the range of 70–130 nm, there were clearly some bigger particles.

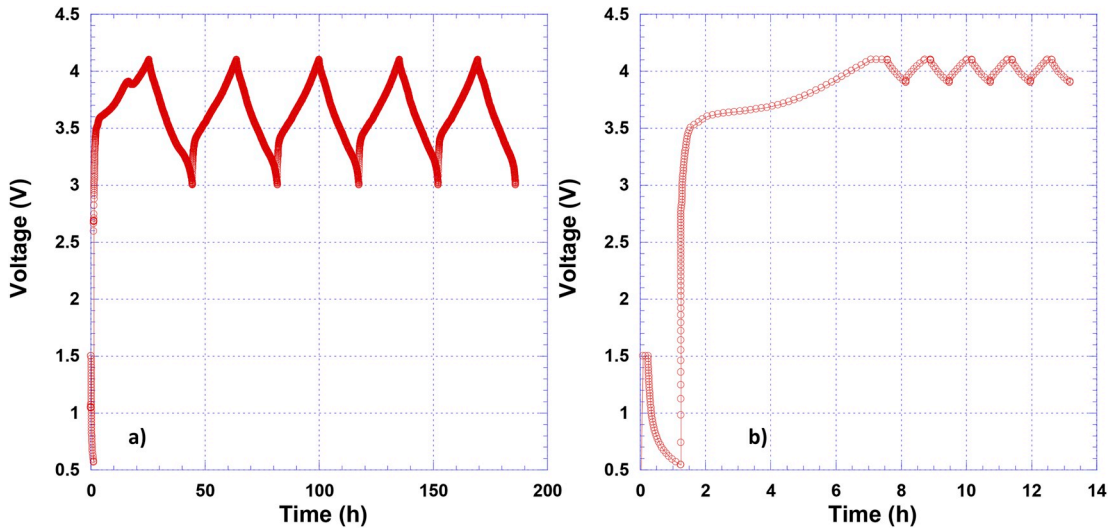

Fig. 2. Voltage curves of a) slow and b) fast formation protocols.

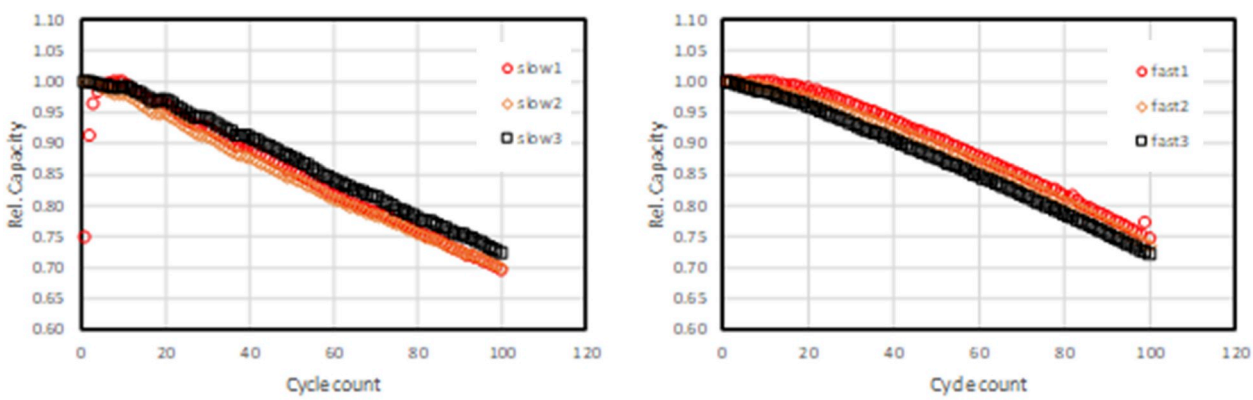

a

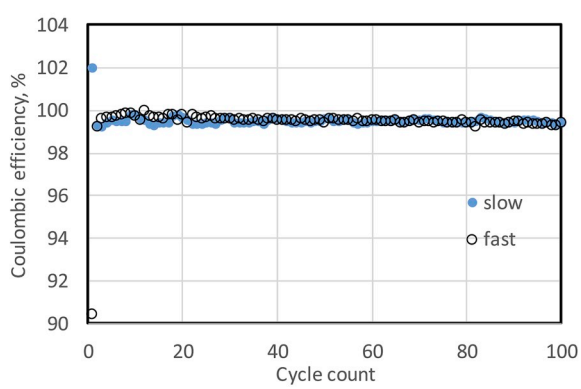

b

Fig. 3. (a). Relative capacity vs. cycle count for cells formed using the slow and fast protocols. It is not known why the first slow protocol cell started at a relatively low capacity and recovered.(b). Coulombic efficiency vs. cycle count for cells formed using the slow and fast protocols.

3.1. Cell performance

Fig. 2 shows the voltage curves for the slow and fast formation protocols, requiring 186 and 13.2 h, respectively. Fig. 3a and b show the electrochemical performance of the cells tested. Fig. 3a shows that, for both protocols, the capacity fade with time is approximately linear, and the apparent fade rate is very close. The slopes of the lines in Fig. 3a indicate that the relative capacities decrease (1σ) by 3.03×10^{-3} (7.02×10^{-5}) per cycle for the slow formation cells and by 2.81×10^{-3} (1.33×10^{-4}) per cycle for the fast ones. These values indicate that the fast protocol can maintain approximately the same (±1σ) fade rate while reducing the formation time to 7% of the slow one.

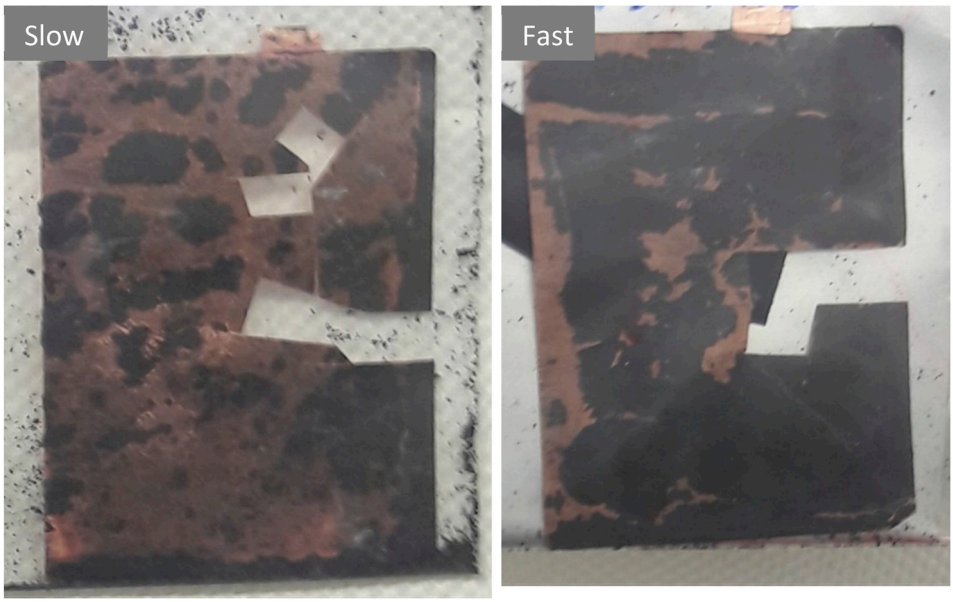

Fig. 4. Glove box images of the Si-graphite anodes after cycling. The holes in the anode laminates are from sampling for XPS and SEM analysis.

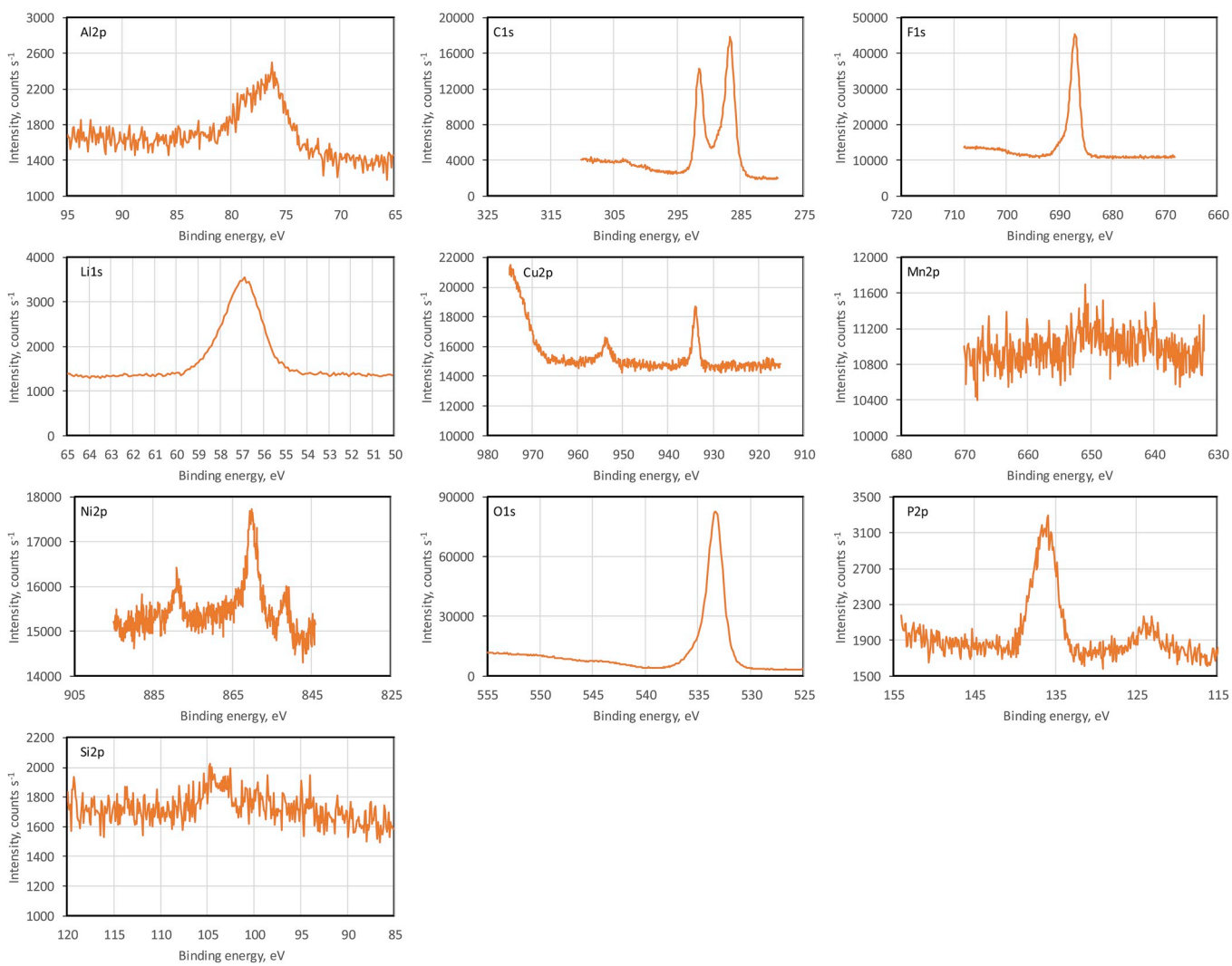

Fig. 5. (a). XPS results from the slow protocol anode surface after aging.(b). XPS results from the fast protocol anode surface after aging.

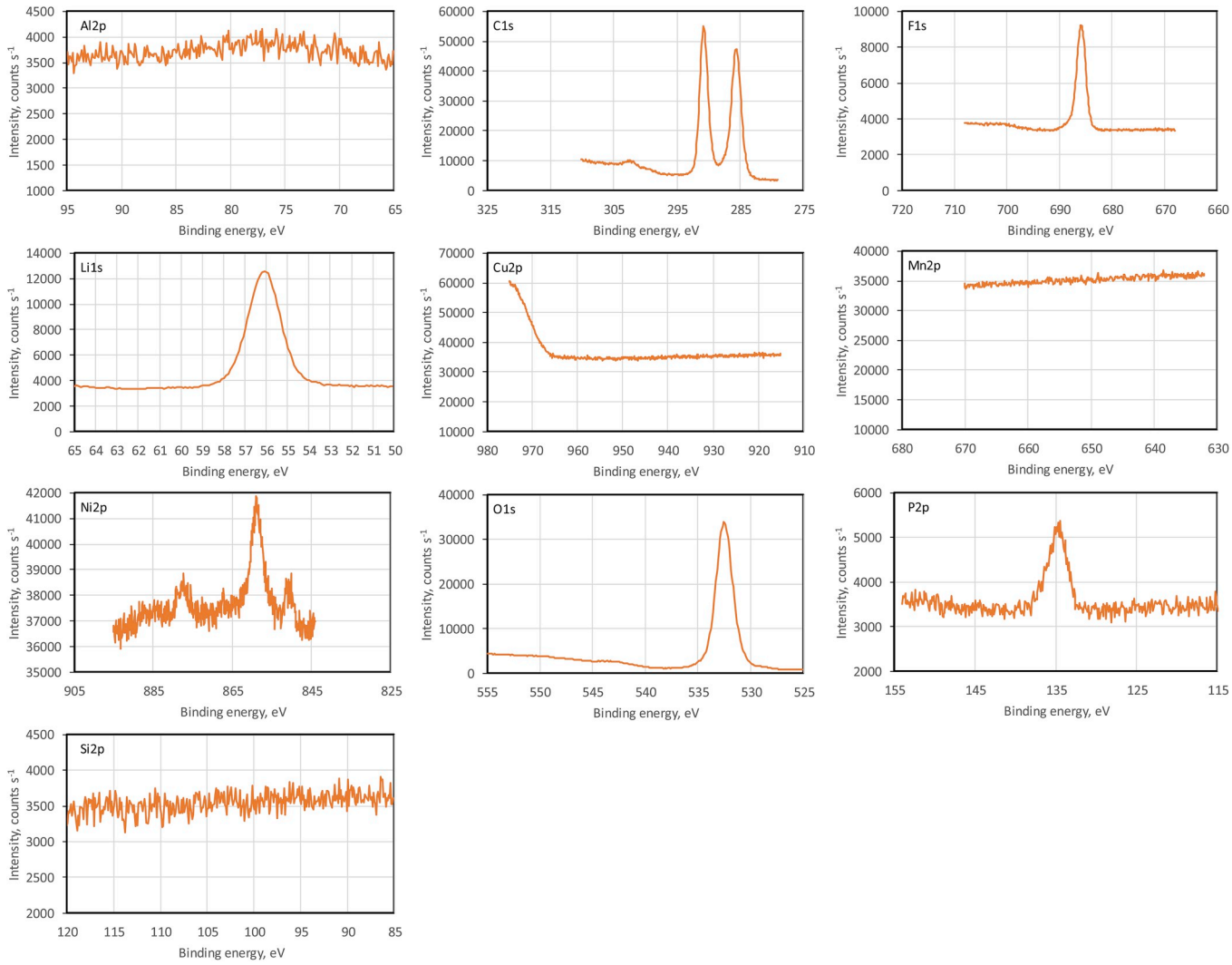

Fig. 5. (*continued*).

Table 2
Composition of surface material on the anodes.[a]

Formation	Composition, at.%								
	C	O	Li	F	P	Ni	Al	Cu	Si
Slow	24.41	29.59	29.78	11.58	1.59	0.28	2.06	0.20	0.52
Fast	22.94	36.67	33.53	5.83	0.54	0.15	0.32	0.00	0.00

[a] The average, estimated uncertainty is ~10% of the value reported.

Fig. 3b shows the change in coulombic efficiency of the cells with cycle number. After a few initial cycles, the coulombic efficiency of cells from both formation protocols was greater than 99%. The data in Fig. 3b show virtually identical plots for the two protocols.

3.2. Post-test examination

After cycling, the cells were opened and examined in an argon-filled glove box. Fig. 4 shows images of the aged Si-graphite anodes. The active material was easily delaminated from the current collector for both formation protocols during disassembly and careful handling, with more material coming off from the slowly formed anode.

3.2.1. X-ray photoelectron spectroscopy

Fig. 5a and b show XPS results in selected ranges of binding energies. From these figures, similarities and differences are apparent. For example, the C1s spectra indicate two carbon environments in both samples, consistent with C-C and C-H environments (~285 eV) and C-F or Li_2CO_3 environments (~289–290 eV) [22,23]. Of more interest are the presence of Al and Cu in the slow formation anode, the presence of Ni in both anodes, and the absence of Si in the fast formation anode.

The presence of Cu and Al in the Si electrode may indicate corrosion of the underlying foil in the electrodes. In the case of Al, this would start at the cathode and migrate across the cell. However, it is intriguing that Cu and Al were found in only the slow formation anode. The slow formation process may be sufficient time for, for example, the copper foil to corrode because it was at a relatively high potential at low states of charge for a longer period than would have occurred at the fast rate.

The apparent absence of Si in the anode from the fast protocol may indicate that the SEI layer had become very thick. Such an SEI layer

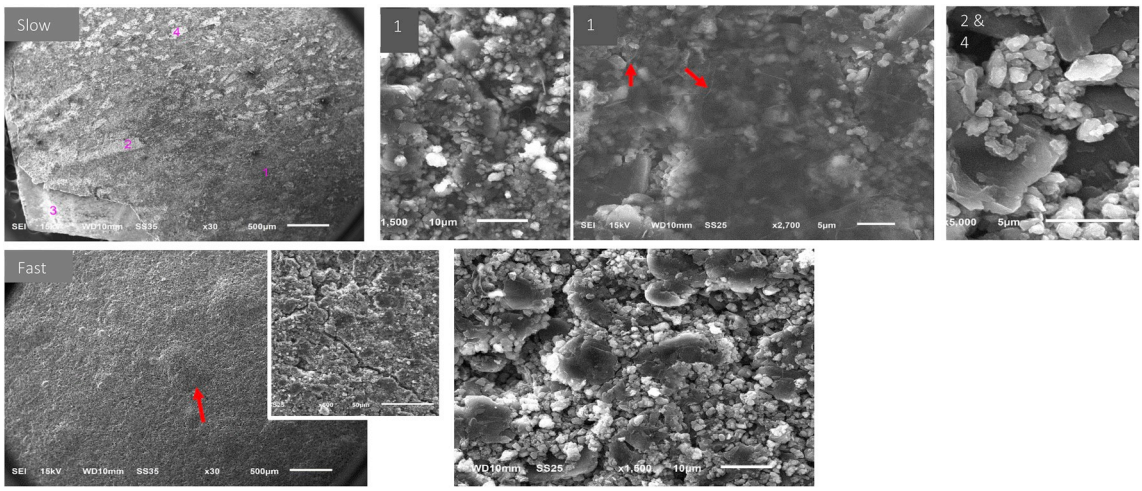

Fig. 6. Scanning electron micrographs of anodes formed with the slow and fast protocols. The results from the slow formation are given in the top row, and those from the fast protocol, on the bottom. The red arrows indicate features of interest that are discussed in the text. (For interpretation of the references to colour in this figure legend, the reader is referred to the Web version of this article.)

could prevent observation of the underlying materials because XPS can measure only the top few nanometers of a material. Material below a thick layer may thus not be detected by XPS.

The results shown in Fig. 5a and b were converted into concentrations of the respective elements and are given in Table 2. As evident from the data, the concentrations of F, P, Ni, and Al are about two times (or more) higher on the anode from the slow than fast protocol. This could be due to a greater amount of electrolyte decomposition on the slow protocol anode. Interestingly, based on the F1s spectra in Fig. 5a and b, all the fluorine may be present as LiF. Combining this observation with the F composition data in Table 2 indicates about twice the amount of LiF in the slow protocol cell. Additionally, from those figures, one can see that there are two phosphorus environments in the slow protocol cell and only one in the fast protocol cell.

3.2.2. Scanning electron microscopy

Selected areas of the two types of anodes were examined under a scanning electron microscope (see Fig. 6). The anode surface from the slow process had a mottled appearance. The darker area (#1 in top row of Fig. 6) was covered with a thin film (red arrows). The lighter areas (#2 and 4) did not show a film, which may have come off onto the separator during disassembly.

The surface from the fast protocol anode surface had large bubbles (see red arrow in bottom row of Fig. 6), indicating gas buildup. Cracks were seen on top of bubbles (inset). The active layer had better adherence to the current collector than the slow protocol active layer.

4. Discussion

The above results indicate that the performance of the fast and slow protocol cells is about the same. In particular, the capacity fade rates were about the same, and the coulombic efficiencies were very similar and did not change appreciably with cycle number. Together, these indicate that the SEI layer in both cases was stable and functioned similarly.

The XPS data indicate that the composition of the SEI layers is different for the two protocols. There was more LiF and more phosphorus-containing phases in the slow than in the fast case, indicating a greater amount of decomposition of $LiPF_6$ on the graphite surface. Apparently, this difference did not change the capacity fade rates of the cells. The difference may impact the cell impedance, though. The change in impedance was beyond the scope of this study.

The microstructure of the two types of SEI layer was similar. The difference in surface chemistry may show that, in this case, the layers form in a similar fashion, regardless of chemistry.

Given the difference in time that the two processes take, the fast protocol may provide a more economical path, making silicon-graphite anodes more attractive for vehicle applications.

5. Conclusion

The effect of formation protocol was investigated in small pouch cells containing silicon-graphite/$Li(Ni_{0.5}Mn_{0.3}Co_{0.2})O_2$ chemistry. Both the slow and fast formation protocols yielded cells with similar performance characteristics. The SEI layers in both cells, even though different in chemistry, were stable and functioned analogously. The fast protocol may thus provide a more economical route to cell fabrication.

Acknowledgments

We gratefully acknowledge support from the U.S. Department of Energy, Vehicle Technologies Office. Argonne National Laboratory is operated for DOE Office of Science by UChicago Argonne, LLC, under contract number DE-AC02-06CH11357.

The work at Oak Ridge National Laboratory, managed by UT Battelle, LLC, for the U.S. Department of Energy under contract DE-AC05-00OR22725, was sponsored by the Office of Energy Efficiency and Renewable Energy, Vehicle Technologies Office, Applied Battery Research.

The U.S. government retains for itself, and others acting on its behalf, a paid-up nonexclusive, irrevocable worldwide license in said article to reproduce, prepare derivative works, distribute copies to the public, and perform publicly and display publicly, by or on behalf of the government.

References

[1] M.D. Radin, S. Hy, M. Sina, C. Fang, H. Liu, J. Vinckeviciute, M. Zhang, M. S. Whittingham, Y.S. Meng, A. Van der Ven, Narrowing the gap between theoretical and practical capacities in Li-ion layered oxide cathode materials, Adv. Energy Mater. (2017) 1602888.

[2] K.G. Gallagher, S.E. Trask, C. Bauer, T. Woehrle, S.F. Lux, M. Tschech, P. Lamp, B. J. Polzin, S. Ha, B. Long, Q. Wu, W. Lu, D.W. Dees, A.N. Jansen, Optimizing areal capacities through understanding the limitations of lithium-ion electrodes, J. Electrochem. Soc. 163 (2015) A138–A149.

[3] J. Li, Z. Du, R.E. Ruther, S.J. An, L.A. David, K. Hays, M. Wood, N.D. Phillip, Y. Sheng, C. Mao, S. Kalnaus, C. Daniel, D.L. Wood, Toward low-cost, high-energy density, and high-power density lithium-ion batteries, JOM (J. Min. Metals Mater. Soc) 69 (2017) 1484–1496.

[4] M.T. McDowell, S.W. Lee, W.D. Nix, Y. Cui, Understanding the lithiation of silicon and other alloying anode for lithium-ion batteries, Adv. Mater. 25 (2013) 4966–4984.
[5] J. Bareño, I.A. Shkrob, J.A. Gilbert, M. Klett, D.P. Abraham, Capacity fade and its mitigation in Li-ion cells with silicon-graphite electrodes, J. Phys. Chem. C 121 (2017) 20640–20649.
[6] H. Wu, G. Chan, J.W. Choi, I. Ryu, Y. Yao, M.T. McDowell, S.W. Lee, A. Jackson, Y. Yang, L.B. Hu, Y. Cui, Stable cycling of double-walled silicon nanotube battery anodes through solid-electrolyte interphase control, Nat. Nanotechnol. 7 (2012) 309–314.
[7] S. Fang, L. Shen, G. Xu, P. Nie, J. Wang, H. Dou, X. Zhang, Rational design of void-involved Si@TiO_2 nanospheres as high-performance anode material for lithium-ion batteries, ACS Appl. Mater. Interfaces 6 (2014) 6497–6503.
[8] K. McCormac, I. Byrd, R. Brannen, B. Seymour, J. Li, J. Wu, Preparation of porous Si and TiO_2 nanofibres using a sulphur-templating method for lithium storage, Phys. Status Solidi 212 (4) (2015) 877–881.
[9] K. Hays, B. Key, J. Li, D.L. Wood, G. Veith, Si oxidation and H_2 gassing during aqueous slurry preparation for Li-ion battery anodes, J. Phys. Chem. C 122 (2018) 9746–9754.
[10] C. Xu, F. Lindgren, B. Philippe, M. Gorgoi, F. Bjorefors, K. Edstrom, T. Gustafsson, Improved performance of silicon anode for Li-ion batteries: understanding the surface modification mechanism of fluoroethylene carbonate as an effective electrolyte additive, Chem. Mater. 27 (2015) 2591–2599.
[11] S.J. An, J.L. Li, C. Daniel, H.M. Meyer, S.E. Trask, B.J. Polzin, D.L. Wood, Electrolyte volume effect on electrochemical performance and solid electrolyte interphase in Si-graphite/NMC lithium-ion pouch cells, ACS Appl. Mater. Interfaces 9 (2017) 18799–18808.
[12] S.J. An, J. Li, C. Daniel, D. Mohanty, S. Nagpure, D.L. Wood, The state of understanding of the lithium-ion-battery graphite solid electrolyte interphase (SEI) and its relationship to formation cycling, Carbon 105 (2016) 52–76.
[13] K.W. Schroder, H. Celio, L.J. Webb, K.J. Stevenson, Examining solid electrolyte interphase formation on crystalline silicon electrodes: influence of electrochemical preparation and ambient exposure conditions, J. Phys. Chem. C 116 (2012) 19737–19747.
[14] V. Etacheri, O. Haik, Y. Goffer, G.A. Roberts, I.C.I.C. Stefan, R. Fasching, D. Aurbach, Effect of fluoroethylene carbonate (FEC) on the performance and surface chemistry of Si-nanowire Li-ion battery anodes, Langmuir 28 (2012) 965–976.
[15] D.L. Wood, J. Li, C. Daniel, Prospects for reducing the processing cost of lithium ion batteries, J. Power Sources 275 (2015) 234–242.
[16] C. Mao, S.J. An, H.M. Meyer III, J. Li, M. Wood, R.E. Ruther, D.L. Wood, Balancing formation time and electrochemical performance of high energy lithium-ion batteries, J. Power Sources 402 (2018) 107–115.
[17] S.J. An, J. Li, Z. Du, C. Daniel, D.L. Wood, fast formation cycling for lithium ion batteries, J. Power Sources 342 (2017) 846–852.
[18] J. Li, C. Rulison, J. Kiggans, C. Daniel, D.L. Wood III, Superior performance of $LiFePO_4$ aqueous dispersions via corona treatment and surface energy optimization, J. Electrochem. Soc. 159 (2012) A1152–A1157.
[19] K.A. Hays, R.E. Ruther, A.J. Kukay, P. Cao, T. Saito, D.L. Wood, J. Li, What makes lithium substituted polyacrylic acid a better binder than polyacrylic acid for silicon-graphite composite anodes? J. Power Sources 384 (2018) 136–144.
[20] J. Li, C. Daniel, S.J. An, D.L. Wood, Evaluation of residual moisture in lithium-ion battery electrodes and its effect on electrode performance, MRS Advances 1 (15) (2016) 1029–1035.
[21] J.Y. Howe, L.A. Boatner, J.A. Kolopus, L.R. Walker, C. Liang, N.J. Dudney, C. R. Schaich, Vacuum-tight sample transfer stage for a scanning electron microscopic study of stabilized lithium metal particles, J. Mater. Sci. 47 (2012) 1572–1577.
[22] From NIST database B.V.R. Chowdari, K.F. Mok, J.M. Xie, R. Gopalakrishan, Solid State Ionics 76 (1995) 189.
[23] From NIST database S. Contarini, J.W. Rabalais, J. Electron. Spectrosc. 35 (1985) 191.